AerospaceEurope Conference2021
WARSAW, POLAND | 23 -26 NOVEMBER 2021
CEAS Council of European Aerospace Societies

# EFFECTS OF FREESTREAM DISTURBANCES IN FRONT OF SPIKED BLUNT NOSE AT HYPERSONIC FLOW

Ashish Vashishtha[1,*], Shashank Khurana[2,*], Dean Callaghan[3] & Cathal Nolan[1]

[*]Joint First Authors
[1]Department of Aerospace and Mechanical Engineering, Institute of Technology Carlow, IRELAND.
[2]Department of Mechanical Engineering, BITS Pilani, Dubai Campus UAE.
[3]The Centre for Research & Enterprise in Engineering (engCORE), Institute of Technology Carlow, IRELAND.

## Abstract

The effects of high frequency slow and fast acoustic wave freestream disturbances are modelled in front of pulsating bow shock formed at spiked blunt nose in hypersonic flow. These disturbances are introduced as time-dependent inflow boundary condition with pressure fluctuation amplitudes of up to 1% at a single frequency of 20 kHz. In this study, initially spiked blunt nose exhibiting pulsating flow field in front of spiked blunt nose ($L/D = 2$) at hypersonic flow Mach 6, has been simulated by using 2D axisymmetric Navier Strokes Laminar solver. Different freestream disturbances are introduced after achieving self-sustainable pulsating flow and replaced with constant boundary condition after 2 ms. The stabilization of the large amplitude pulsations are observed by fast acoustic disturbances with pressure amplitude of more than 0.5% and & 1%, while slow acoustic wave disturbance can stabilize the pulsation only with 1% pressure fluctuations.

**Keywords:** Numerical Simulation, Acoustic Disturbances, Hypersonic, Pulsation, Flow Control

## 1. Introduction

This study is motivated to understand the effectiveness of the freestream disturbance as, active flow control methods, to manipulate the pulsating flow field associated with shockwaves at high-speed flows. The large amplitude bow shock fluctuations are observed in variety of flow control methods tested in test-sections of supersonic and hypersonic wind tunnels. The spike attached to flat surface cylindrical blunt nose exhibits these large amplitude shock instabilities as observed in wind tunnel test-sections in high-speed flows [1, 2]. The numerical simulations [3, 4] explains the mechanism causing these bow-shock fluctuations in pulsation and oscillation modes. Similarly, bow shock in front of blunt nose with concave hemispherical shell at hypersonic wind tunnel test section shows non-linear, large amplitude fluctuations with intermittent [5, 6] transitions from large amplitude fluctuations to small amplitude shock fluctuations and vice versa. The supersonic counter-jet flow as an active drag control technique in front of blunt nose at hypersonic flow, is also subjected to large amplitude fluctuations in case of long penetration mode and remain stable in short penetration mode [7].
High-speed wind tunnels test-sections inherently consists of disturbances due to various different systems attached to it. The eddy-Mach-wave acoustic radiation from the turbulent boundary layer in nozzle wall of supersonic/hypersonic wind tunnel can produce variety of acoustics disturbances in test-section. A very small nozzle throat area in case of high-supersonic and hypersonic nozzle may cause vortical disturbances along the centerline of test-section. If the stagnation flow is heated before travelling through the nozzle by various means, it can also lead to entropy disturbances in test-section. Random particles may appear in the test-section from either heating source or rust present at the wall of nozzle inlet. Vashishtha [8] has captured small vortical disturbances using high-speed camera (with 50k fps), which causes gradual initiation of non-linear bow-shock instabilities in front

of hemispherical shell at hypersonic Mach 7. Also, the bow-shock disturbance caused by random particles in flow may lead to abrupt transition to large amplitude bow-shock disturbances and vice versa. Although, the presence of various high-level freestream disturbances compared to the flight level, in high-supersonic and hypersonic wind tunnels was understood early and has been known since 1950s. The operational quiet wind tunnels are developed in recent decades [9], in order to understand long standing problem of laminar to turbulent transition in hypersonic boundary layer [10]. However, the disturbances may not affect the performance measurement in wind tunnel condition for stable flow. But, without estimation and understanding of freestream disturbances, the studies of unsteady phenomenon in high supersonic or hypersonic flow may produce very different results when conducting same tests in various wind tunnels and may also lead to different outcomes far from the flight.

This study focuses on large amplitude bow-shock instabilities observed in front of spiked flat-faced cylindrical blunt nose in hypersonic flow. A spiked blunt nose in supersonic and hypersonic flow is considered an effective drag reduction technique. [11] However, the flow-field in front of a spiked blunt nose is subjected to small amplitude oscillations and large amplitude pulsation fluctuations. Similar unstable flow-field characteristics can also be observed, while unstart of air breathing engines, due to unstable bubble creation on the ramp before inlet [12]. The recent numerical studies showed that the pulsation mode fluctuations in front of flat-face blunt nose with spiked body can be controlled either by making small changes in the geometry passively or freestream flow, which can lead to stabilized bow-shock [13, 14] in hypersonic flow. In case of concave hemispherical shell, the experiments carried out in hypersonic wind tunnel shows that the non-linear bow shock large amplitude fluctuations are effectively controlled by providing small passive control in form of spike within the cavity at the center or crosswire along the diameter of cavity[15]. The injection of light gases in counter-jet flow was studied with motivation to provide bow-shock control [16, 17] in long penetration mode. As the small change in geometry can provide the stabilization effects to bow shock, it is hypothesized that a small disturbance in freestream can also provide the stabilization effect. With the motivation to actively control the large amplitude bow shock fluctuations by introducing disturbances at spatial locations in the domain, this study lays down the preliminary work to develop an understanding of attenuation of freestream disturbances in front of a spiked blunt nose of ($L/D = 2$), where $L$ is length of spike and $D$ is diameter of the cross-section of blunt nose at hypersonic Mach number 6 using numerical simulations. The main objectives are defined as follows: 1) to model the acoustic freestream disturbances in front of spiked blunt nose, and 2) to understand the flow control mechanism of freestream disturbances in manipulating the unsteady flow-field.

## 2. Numerical Method

The numerical simulations are performed for a flat-face cylindrical blunt nose ($D = 40$ mm) with a single spike ($d/D =$ 0.1) of length $L = 2D$ attached at the center of nose in hypersonic flow. Here, $D$ is diameter of the cross-section of cylindrical blunt nose and $d$ represents the diameter of the cross-section of cylindrical spike. is the The two-dimensional axi-symmetric unsteady Navier-Stokes equations are solved for compressible laminar hypersonic Mach number 6. The solver uses Lious all-speed AUSM (Advection Upstream Splitting Method) + up scheme [18] with upwind biased third order MUSCL (monotonic upstream-centered scheme for conservative laws) interpolation for computing the spatial inviscid fluxes. The second order central difference scheme is used for computing viscous fluxes as well as source terms (because of axi-symmetry). The explicit third order TVD Runge-Kutta Method[19] is used for time integration. The solver with constant boundary conditions is already validated in recent study [14] by comparing previous experimental data as well as appropriate grid size and time-step is selected to achieve grid independent unsteady solution. In the current study, additionally time-dependent inflow boundary conditions were modelled to understand the effects of fast ($u + c$) and slow ($u - c$) acoustic disturbances.

### 2.1 Computational Domain:

Figure 1a shows the overall computational domain and boundary conditions used. Fig. 1b shows the generated structured grid of size $201 \times 121$ for spike of length $L/D = 2.0$ with minimum grid size near the wall as 2 $\mu m$. The disturbance free inflow condition has been modelled at Mach 6 hypersonic

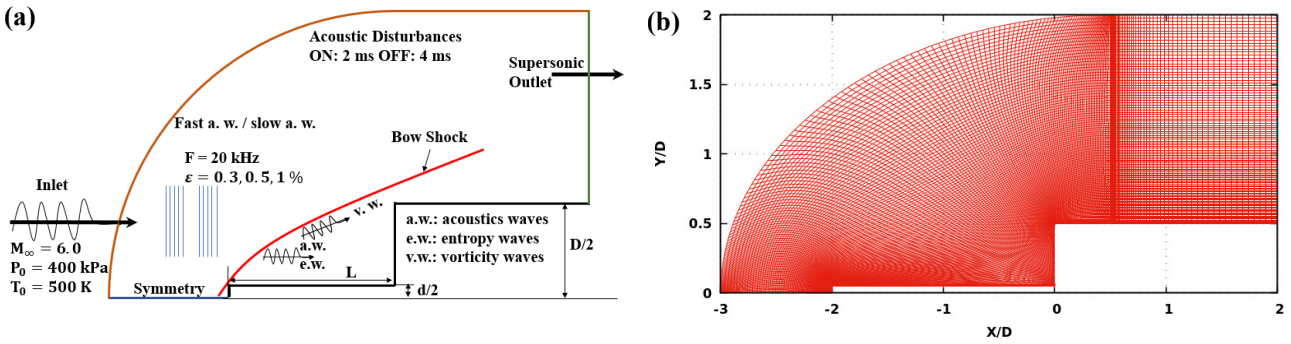


Figure 1 – (a) Computational domain with boundary conditions (b) Computational grid of size $201 \times 121$ used for simulations.

Table 1 – VKI H3 hypersonic wind tunnel test-section conditions [2]

| Property | Specification |
|---|---|
| Mach Number ($M_\infty$) | 6.0 |
| Stagnation Pressure ($P_0$) | 400 kPa |
| Stagnation Temperature ($T_0$) | 500 K |
| Wall Temperature ($T_w$) | 300 K |
| Reference Length ($D$) | 40 mm |
| Reynolds Number ($Re$) | $0.134 \times 10^6$ |

flow with stagnation pressure 400 kPa and stagnation temperature 500 K, similar to VKI Hypersonic Wind Tunnel H3 test-section [2] as listed in Table 1. At the wall, no-slip boundary condition with an isothermal wall temperature of 300 K is assumed. The outlet is modelled as supersonic outlet. The simulation starts as impulse start and 5-6 pulsating cycles are observed within 2 ms. In all the computations, freestream (FS) disturbances are switched on at time $t = 2$ ms and switched off at time $t = 4$ ms. The simulation was continued for next 2 ms with constant boundary condition again. The computation has been performed for total 6 ms with a constant physical time-step of $1 \times 10^{-9}$ sec. The flow is initialized by submerging spiked body with low speed flow (100 m/s) and using impulse start, hypersonic flow from inlet at time, $t = 0$.

## 2.2 Freestream Disturbances:

The high frequency freestream disturbances with single frequency 20 kHz are modelled [20] with time-dependent inlet boundary conditions. The instantaneous values of any disturbances in freestream parameters are modelled with following equation:

$$\begin{bmatrix} u' \\ v' \\ p' \\ T' \end{bmatrix}_\infty = \begin{bmatrix} \bar{u} \\ \bar{v} \\ \bar{p} \\ \bar{T} \end{bmatrix}_\infty + \begin{bmatrix} |u|' \\ |v|' \\ |p|' \\ |T|' \end{bmatrix}_\infty e^{i[k_x(x-a)+k_y(y-b)-\omega t]} \tag{1}$$

where, $u$, $v$, $p$ and $T$ are non-dimensional $x$-direction velocity, $y$-direction velocity, pressure and temperature, respectively at any location $(x, y)$ in the domain. The subscript $_\infty$ denotes free stream condition at inlet boundary. The superscript $'$ denotes instantaneous time-dependent parameter, while the $(\bar{})$ represents the mean parameter, which are derived from test-section condition in Table 1. The location $(a, b)$ assumed to be the source of acoustic disturbances, is considered at (-6, 0) far from the inlet boundary. The amplitudes, wave number vector and non-dimensional frequency are modelled

as follows:

$$\begin{aligned} |p^{'}| &= \varepsilon, & |u^{'}| &= \pm\varepsilon M_\infty cos\theta, \\ |T^{'}| &= \varepsilon(\gamma-1)M_\infty^2, & |v^{'}| &= \mp\varepsilon M_\infty sin\theta, \\ k_x &= k_\infty cos\theta, & k_y &= -k_\infty sin\theta, \\ k_\infty &= \frac{\omega}{cos\theta \pm 1/M_\infty}, & \omega &= \frac{2\pi F L_{ref}}{v_{ref}} \end{aligned} \tag{2}$$

here, $\theta$ is angle of incidence of acoustic disturbances with respect to perpendicular to axial direction, for two-dimensional wave ($\theta$ =0 degrees, in all calculations). The non-dimensional pressure fluctuation amplitude or wave amplitude is characterised as small parameter $\varepsilon$, and the amplitudes of other non-dimensional parameters are dependent on that. $k_x$ and $k_y$ are $x$-direction and $y$-direction wave vector components, respectively and $k_\infty$ is absolute wave number. $F$ is frequency of disturbance and $\omega$ is non-dimensional angular frequency dependent on that. In case of $\pm$ and $\mp$ signs in relevant component, the top sign represents the fast moving acoustic wave and the bottom sign represents for slow moving acoustic waves. The fast and slow acoustic wave disturbances for given conditions ($\theta$ =0 degrees) are derived from below:
Fast Acoustic Wave Disturbances:

$$|p^{'}| = \varepsilon, \quad |u^{'}| = \varepsilon M_\infty, \quad |v^{'}| = 0, \quad |T^{'}| = \varepsilon(\gamma-1)M_\infty^2 \tag{3}$$

Slow Acoustic Wave Disturbances:

$$|p^{'}| = \varepsilon, \quad |u^{'}| = -\varepsilon M_\infty, \quad |v^{'}| = 0, \quad |T^{'}| = \varepsilon(\gamma-1)M_\infty^2 \tag{4}$$

The effects of acoustic wave disturbances are simulated for non-dimensional pressure amplitude of $\varepsilon = 0.3$, $0.5$ and, $1$% for both slow and fast acoustic waves. The absolute wave number ($k_\infty$) for slow and fast acoustic waves used for computation are 6.42 and 4.26, respectively.

## 3. Results & Discussions

The spiked blunt nose of length-to-diameter ratio $L/D = 2$ is simulated for a time duration of 6 ms at hypersonic Mach number 6 at 400 kPa stagnation pressure and 500 K stagnation temperature initially. The time-dependent drag coefficient variation has been computed at each 1 $\mu s$ along with the non-dimensional pressure at location $y = D/4$ on the flat-face of the blunt nose. The results are analyzed by comparing the time-history of drag coefficient as well as Mach contours at a particular time-stamp. Furthermore, the Fast Fourier Transform (FFT) plots of pressure were used to describe the control of bow shock fluctuations.

### 3.1 Undisturbed flow

Figure 2 shows the time history of time dependent drag coefficient for the simulated spiked body in hypersonic flow, subjected to various amplitude fast acoustic wave disturbances with 20 kHz frequency, modelled at inlet boundary. The simulated pressure amplitudes are $\varepsilon$ = 0.0, 0.3, 0.5 and 1.0. Here, $\varepsilon$ = 0.0 represents the undisturbed flow throughout 6 ms. The undisturbed flow exhibits large amplitude pulsations in bow shock, which result in time-dependant large variation in pressure on the spiked blunt body, causing fluctuating drag between value up to 2-3. The drag coefficient vary in similar manner for the undisturbed flow with low frequency for all the duration of simulation. These self-sustainable pulsation can be explained from Mach contours shown in the Fig 3a undisturbed flow. The pulsation in bow shock in front of the spiked body with flat-face in hypersonic flow are explained by three processes: inflation, withheld and collapse [3, 13]. The bow shock initially establish itself in front of the spike and when interacts near the corner of the flat-faced blunt body, a triple point is formed due to interaction from the spike shock and afterbody shock. The lateral movement of triple point and interaction with corner, reflects three maxima in single pulsation peak (in Fig. 2). The upper image in Fig 3a shows the Mach contours at maximum drag at time, $t$ = 0.87 ms. The air gets compressed near the spike root region and with lateral movement of triple point, compressed air starts expanding, which initiates the inflation process. The high pressure region at the root gather the incoming mass due to recirculation and larger vortex is formed, which pushes the bow shock upstream

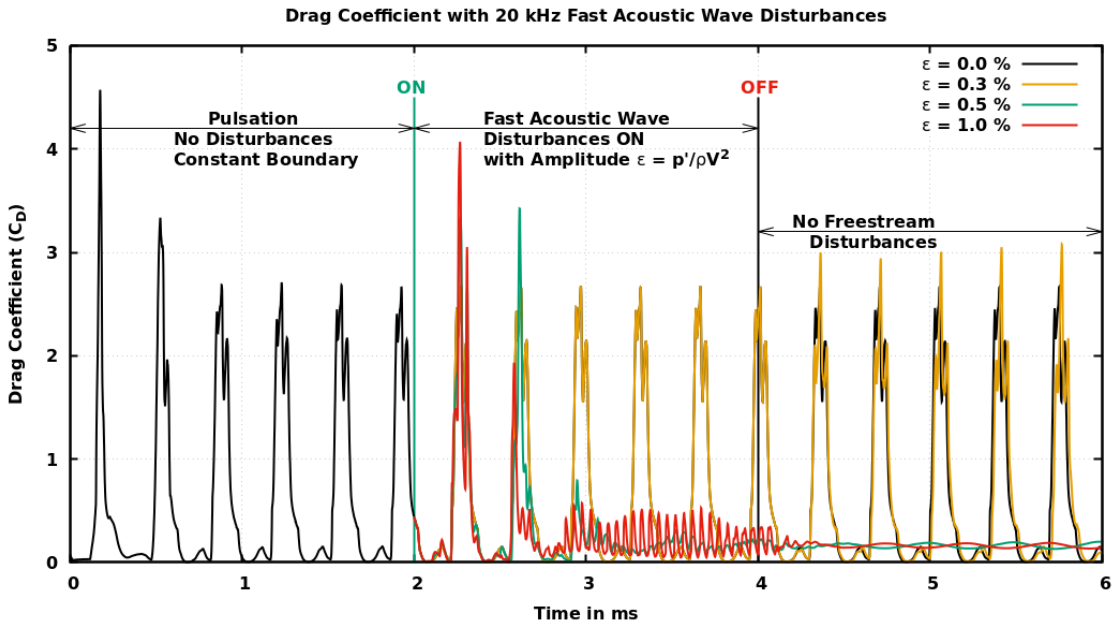


Figure 2 – Time history of drag coefficient with fast acoustic wave disturbances of various amplitudes $t$ =0 to 2 ms, with constant boundary conditions, disturbance ON between $t$ =2 to 4 ms, and disturbance OFF for time, $t$ = 4 ms onward

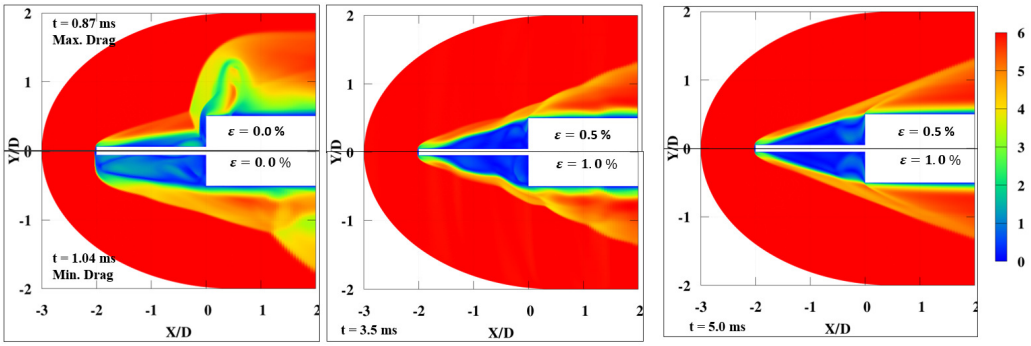


(a) No Disturbances (b) While Disturbances ON (c) Post Disturbance

Figure 3 – Mach number contours, (a) maximum and minimum drag configuration (for $\varepsilon$ =0.0), (b) instantaneous effect of disturbances with $\varepsilon$ =0.5 and 0.1), (c) post disturbance stable flow.

as well as inflate the bow shock laterally. The bottom image in Fig. 3a, shows the Mach contours at minimum drag flow field, time $t$ = 1.04 ms. After the maximum upstream movement of bow shock, further expansion in lateral direction occur, which is the withheld process. During lateral expansion, some mass starts slipping from the corner of blunt nose, causing low pressure in spike root region, which initiates the collapse phase. With time, large mass skips near the corner of blunt nose and the collapse phase ends when the bow shock reaches near the corner in angular manner. There is always a mass imbalance remaining, which continues the pulsation in self-sustainable manner.

## 3.2 Effect of Fast Acoustic Waves

The effects of introducing fast acoustic waves disturbance on pulsation of bow shock are shown in Fig. 2 with $\varepsilon$ = 0.3, 0.5 and 1.0% with 20 kHz frequency. The disturbances are switched on between time, $t$ = 2 ms to 4 ms. Between time, $t$ = 4 ms to $t$ = 6 ms, the incoming flow remain undisturbed again as the undisturbed flow shows the pulsation throughout the time along with the case of $\varepsilon$ = 0.3%. When this low amplitude fast acoustic disturbance interacts with the bow shock, it doesn't affect it's pulsation at all, however, when the disturbance is removed, there is slight change in dynamics of triple point movement near the corner, which can be seen as a slight shift in three maxima in the single pulsation peak after time, $t$ = 4 ms. Overall, the $\varepsilon$ = 0.3% fast acoustic disturbances doesn't alter

dynamics of pulsation significantly. However, the fast acoustic wave disturbance with amplitude $\varepsilon =$ 0.5% and 1% lead to complete stabilization of pulsating bow shock in front of spiked body, even after the disturbance is removed at time, $t = 4$ ms. When the fast acoustic wave disturbance is switched on at the inlet boundary, it starts interacting with bow-shock after one and a half pulsation cycle. The high frequency and appropriate amplitude of fluctuations modifies the pulsation by creating ripples in the bow shock as seen in Fig.3b at time, t = 3.5 ms, when the fast acoustic disturbances are still on. Due to interaction of high frequency of acoustic disturbances, these ripples reduces the mass imbalance within bow-shock and front-face, and allows it to settle down by imposing its own frequency. The low frequency and high amplitude fluctuations are turned into high frequency low amplitude fluctuations by redistributing the energy of the system, as the lower amplitude $\varepsilon = 0.5\%$ shows lesser disturbance in bow shock, compared to $\varepsilon = 1.0\%$, when the disturbances are active between $t = 3$ ms to 4 ms as seen in Fig. 2. After the disturbances are switched off, the bow shock remains stable for rest of the simulation time and reflect almost constant drag coefficient less than 0.1 for both the cases of fast acoustic disturbances with amplitude $\varepsilon = 0.5\%$ & 1%. The bow shock stability after the removal of fast acoustic disturbance can be attributed to the hysteresis effect of the overall system, when it attains stability, there is minimal mass imbalance due to stabilised root vortex.

## 3.3 Effect of Slow Acoustic Waves

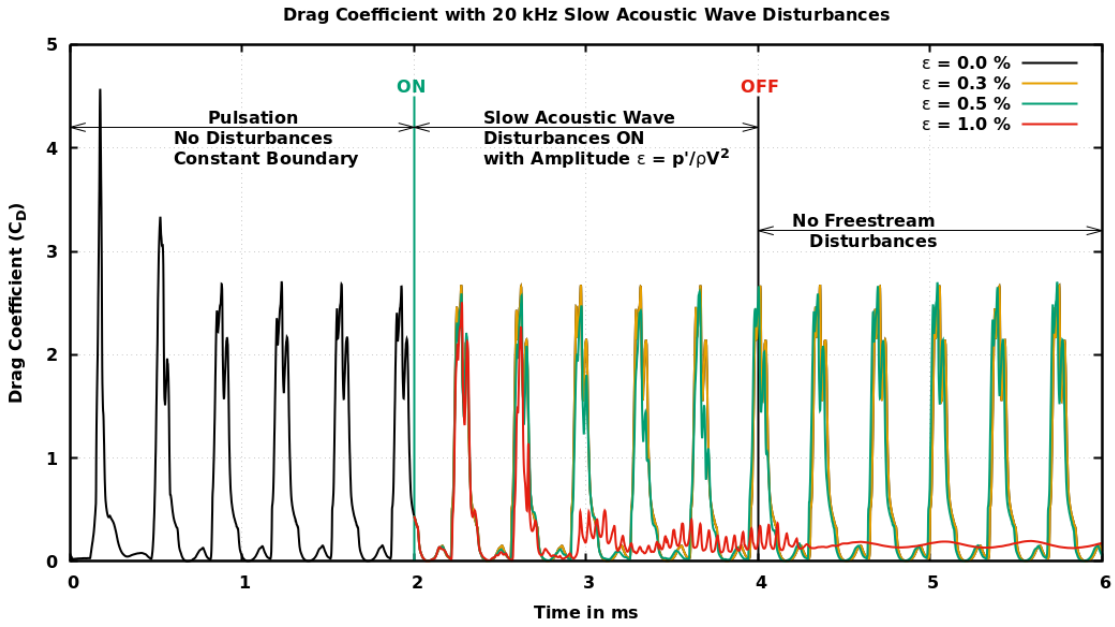


Figure 4 – Time history of drag coefficient with slow acoustic wave disturbances of various amplitudes

Figure 4 shows the time history of drag coefficient of spiked body at simulated hypersonic Mach number. In this case also, the slow acoustic wave disturbances with same amplitudes are switched on between time, $t = 2$ ms to 4 ms and the freestream remain disturbance free for the next 2 ms. The slow acoustic wave disturbance reaches almost 2 pulsation cycles after it switched on. The disturbance amplitude $\varepsilon = 0.3\%$ and 0.5% do not significantly influence the pulsation phenomenon, when the disturbances are on and beyond, when the disturbances are removed. However, the disturbance amplitude $\varepsilon = 1\%$ exhibits the similar effective control as seen in case of fast acoustic wave. This depicts that not only the amplitude and frequency is important in effective control, but also the wave number plays an important role in controlling large amplitude bow shock pulsation. It is also noted that bow shock position, when the acoustic disturbances starts interacting with it, may also lead to different outcome as the fast acoustic wave starts interacting when the bow shock pulsation was in collapse phase, while the slow wave interacts during the witheld phase of the bow shock pulsation.

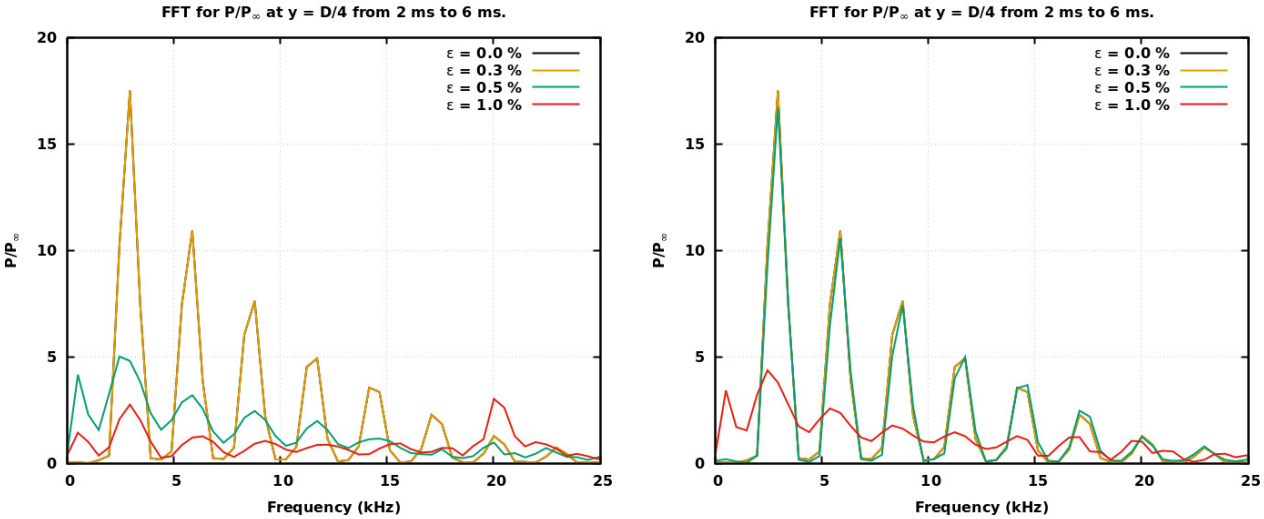


**(a) Fast Acoustic Waves** **(b) Slow Acoustic Waves**

Figure 5 – Time history of drag coefficient with slow acoustic wave disturbances of various amplitudes

### 3.4 Effect on energy distribution

Figure 5 shows the FFT plots obtained from non-dimensional pressure data accumulated at $y = D/4$ on flat-face during 2 ms to 6 ms. Figure 5a shows the FFT plot to understand the effects of fast acoustic disturbances, while Fig. 5b plots shows the effects of slow acoustic disturbances. When the acoustic disturbances with lower strength (amplitude, $\varepsilon$ = 0.3%) can't affect the bow shock pulsations, the amplitude and frequencies in FFT plots doesn't show any significant difference in comparison to $\varepsilon = 0.0$ for both slow and fast waves. As bow shock pulsations are low-frequency phenomenon, the FFT plot for $\varepsilon = 0.0$, shows higher amplitudes in lower frequency regions. In case of interaction of bow shock with fast acoustic disturbances with the amplitudes $\varepsilon = 0.5\%$ & 1%, there is no significant change in dominant frequencies in Fig. 5a, however the peaks are significantly reduced in amplitudes, specially in low frequency range. The fast acoustic disturbances can significantly reduces the amplitudes of low-frequency peaks in FFT (even at strength $\varepsilon = 0.5\%$) than slow acoustic disturbances. In case of slow acoustic disturbances, only disturbance with higher amplitude, $\varepsilon = 1\%$ leads to stable bow shock. The drops in FFT amplitude are significant for slow acoustic disturbances, but lesser than the case of $\varepsilon = 1\%$ for fast acoustic waves. It can be said here that the acoustic disturbances are effective when the higher energy of larger vortices formed between spike, pulsating bow shock and front face of blunt body during pulsation, is distributed in higher frequency of imposing acoustic disturbance by breaking the larger vortex to smaller eddies, which leads to minimise the mass imbalance in the region and leads to stable bow-shock.

## 4. Conclusions

In the current study, the effects of high frequency fast and slow acoustic disturbances have been studied for large amplitude pulsation of bow shock in front of spiked-blunt nose in hypersonic flow by numerical methods. The blunt nose of diameter ($D$) 40 mm with spike length $L = 2D$ have been simulated at Mach 6 test-section conditons according to VKI H3 hypersonic wind tunnel. The large amplitude pulsations are analyzed in case of undisturbed flow. The high frequency (20 kHz) fast acoustic disturbances with non-dimensional pressure amplitudes 0.5% & 1% have been found effective in controlling the pulsations by stabilizing the bow shock through ripple formation and breaking larger vortex in the spike, bow shock and flat-face region to smaller eddies and reducing the mass imbalance. However, the slow acoustic waves were effective in transitioning pulsations to stable flow field only for pressure amplitude $\varepsilon = 1\%$. This study also suggests that the disturbances present in wind-tunnel test-section may not only affect the boundary layer transition, but also various non-linear, time-dependent phenomenon may exhibit different dynamics in various high-speed wind tunnels. It is

always better to quantify the various disturbances in the test-section while conducting such studies.

## Contact Author Email Address

mail to: ashish.vashishtha@itcarlow.ie

## Copyright Statement



## References

[1] Wood C J. Hypersonic flow over spiked cones. *Journal of Fluid Mechanics*, 12, 1961.

[2] Kenworthy M A. *A Study of unstable axisymmetric separation in high speed flows*. Ph.d. thesis, Virginia Polytechnic Institute and State University, 1978. URL http://hdl.handle.net/10919/76093.

[3] Feszty D, Badcock K J, and Richards B E. Driving mechanisms of high-speed unsteady spiked body flows, part i: Pulsation mode. *AIAA Journal*, 42(1):95–106, 2004. doi: 10.2514/1.9034.

[4] Feszty D, Badcock K J, and Richards B E. Driving mechanism of high-speed unsteady spiked body flows, part 2: Oscillation mode. *AIAA Journal*, 42(1):107–113, 2004. doi: 10.2514/1.9035.

[5] Vashishtha A, Watanabe Y, and Suzuki K. Study of shock shape in front of concave, convex and flat arc in hypersonic flow. *JAXA-SP-14-010*, pages 127–132, mar 2015. URL http://id.nii.ac.jp/1696/00003852/.

[6] Vashishtha A, Watanabe Y, and Suzuki K. Study of bow-shock instabilities in front of hemispherical shell at hypersonic Mach number 7. In *45th AIAA Fluid Dynamics Conference*. AIAA 2015-2638, 2015. doi: 10.2514/6.2015-2638.

[7] Shang J S, Hayes J, Wurtzler K, and Strang W. Jet-spike bifurcation in high-speed flows. *AIAA Journal*, 39 (6):1159–1165, 2001. doi: 10.2514/2.1430.

[8] Vashishtha A. *Bow-Shock Instability and its Control in front of Concave shaped Blunt Nose at Hypersonic Mach No. 7*. Ph.d. thesis, The University of Tokyo, 2016. Thesis Number: 12601 A No. 33230.

[9] Schneider S P. Development of hypersonic quiet tunnels. *Journal of Spacecraft and Rockets*, 45(4):641–664, 2008. doi: 10.2514/1.34489.

[10] Lee C and Chen S. Recent progress in the study of transition in the hypersonic boundary layer. *National Science Review*, 6(1):155–170, May 2018. ISSN 2095-5138. doi: 10.1093/nsr/nwy052.

[11] Mahmoud Y.M. Ahmed and Ning Qin. Forebody shock control devices for drag and aero-heating reduction: A comprehensive survey with a practical perspective. *Progress in Aerospace Sciences*, 112:100585, 2020. doi: 10.1016/j.paerosci.2019.100585.

[12] Chang J, Li N, Xu K, Bao W, and Yu D. Recent research progress on unstart mechanism, detection and control of hypersonic inlet. *Progress in Aerospace Sciences*, 89:1–22, 2017. ISSN 0376-0421. doi: 10.1016/j.paerosci.2016.12.001.

[13] Vashishtha A and Khurana S. Pulsating flow investigation for spiked blunt-nose body in hypersonic flow and its control. In *AIAA Scitech 2021 Forum*. AIAA 2021-0839, 2021. doi: 10.2514/6.2021-0839.

[14] Vashishtha A and Khurana S. Novel mechanism of instability control using a tapered spike in hypersonic flow. In *AIAA Aviation 2021 Forum*. AIAA 2021-2543, 2021. doi: 10.2514/6.2021-2543.

[15] Vashishtha A, Watanabe Y, and Suzuki K. Bow-shock instability and its control in front of hemispherical concave shell at hypersonic Mach number 7. *Transaction of the JSASS, Aerospace Technology Japan*, 14 (ists30):121–128, 2016. doi: 10.2322/tastj.14.Pe_121.

[16] Vashishtha A, Callaghan D, and Nolan C. Drag control by hydrogen injection in shocked stagnation zone of blunt nose. *IOP Conference Series: Materials Science and Engineering*, 1024(1):012110, jan 2021. doi: 10.1088/1757-899x/1024/1/012110.

[17] Harmon P., Vashishtha A, Callaghan D, Nolan C, and Deiterding R. Study of direct gas injection into stagnation zone of blunt nose at hypersonic flow. In *AIAA Propulsion & Energy Forum*. AIAA 2021-3529, 2021. doi: 10.2514/6.2021-3529.

[18] Liou M S. A sequel to ausm, part ii: Ausm+-up for all speeds. *Journal of Computational Physics*, 214(1): 137–170, 2006. ISSN 0021-9991. doi: 10.1016/j.jcp.2005.09.020.

[19] Shu C W and Osher S. Efficient implementation of essentially non-oscillatory shock-capturing schemes. *Journal of Computational Physics*, 77(2):439–471, 1988. ISSN 0021-9991. doi: 10.1016/0021-9991(88)90177-5.

[20] Egorov I V, Sudakov V G, and Fedorov A V. Numerical modeling of the receptivity of a supersonic boundary layer to acoustic disturbances. *Fluid Dynamics*, 41(37), 2006. doi: 10.1007/s10697-006-0020-4.